Perovskite Solar Cells

Deutsche Ausgabe: DOI: 10.1002/ange.201500014
Internationale Ausgabe: DOI: 10.1002/anie.201500014

The Significance of Ion Conduction in a Hybrid Organic–Inorganic Lead-Iodide-Based Perovskite Photosensitizer**

Tae-Youl Yang, Giuliano Gregori, Norman Pellet, Michael Grätzel, and Joachim Maier**

Abstract: *The success of perovskite solar cells has sparked enormous excitement in the photovoltaic community not only because of unexpectedly high efficiencies but also because of the future potential ascribed to such crystalline absorber materials. Far from being exhaustively studied in terms of solid-state properties, these materials surprised by anomalies such as a huge apparent low-frequency dielectric constant and pronounced hysteretic current–voltage behavior. Here we show that methylammonium (but also formamidinium) iodoplumbates are mixed conductors with a large fraction of ion conduction because of iodine ions. In particular, we measure and model the stoichiometric polarization caused by the mixed conduction and demonstrate that the above anomalies can be explained by the build-up of stoichiometric gradients as a consequence of ion blocking interfaces. These findings provide insight into electrical charge transport in the hybrid organic–inorganic lead halide solar cells as well as into new possibilities of improving the photovoltaic performance by controlling the ionic disorder.*

The energy conversion process in photovoltaic devices involves two fundamental steps: the absorption of incident photons generating electron–hole pairs and the transport of these carriers to the external load. Strong optical absorption, efficient generation, and transport of electronic charge carriers are essential prerequisites for photovoltaic materials. In this context, metal-halide-based perovskites containing alkyl ammonium (or formamidinium) cations such as $CH_3NH_3PbX_3$ (or $NH_2CHNH_2PbX_3$) (with X = Cl, Br, I) have gained enormous attention thanks to their outstanding optical and electrical transport properties.[1–5] After the first demonstration as photosensitizers in a mesoscopic dye-sensitized solar cell,[6] the optimization of materials, solar cell structure, and fabrication process has soon increased efficiency up to 20.1 %.[7–11]

[*] Dr. T.-Y. Yang, Dr. G. Gregori, N. Pellet, Prof. M. Grätzel, Prof. J. Maier
Max-Planck-Institute for Solid State Research
Heisenbergstraße 1, 70569 Stuttgart (Germany)
E-mail: g.gregori@fkf.mpg.de
s.weiglein@fkf.mpg.de
N. Pellet, Prof. M. Grätzel
Department of Chemistry and Chemical Engineering
Swiss Federal Institute of Technology
Station 6, 1015 Lausanne (Switzerland)

[**] Dr. H. Hoier and A. Fuchs are thanked for XRD and SEM analyses, respectively.

Supporting information for this article is available on the WWW under http://dx.doi.org/10.1002/anie.201500014.

The great success of these halide perovskites is attributed to their outstanding light harvesting and charge carrier collection properties.[3,12] It has been reported that methylammonium ($CH_3NH_3^+$, MA) iodoplumbates show extremely large diffusion lengths (over 1 μm) for both photogenerated electrons and holes,[12] which has been related to high charge carrier mobility and low recombination rates.[13] The far-reaching absence of recombination centers is in agreement with modeling results suggesting the presence of shallow donors and acceptors,[14] although, more recently, it was shown that iodine interstitials may act as deep traps.[15]

A striking feature of these perovskites is their high apparent dielectric constant ε'_r at low frequencies ($\varepsilon'_r = 10^3$, which increased by a factor of 1000 under illumination)[16,17] as well as a distinct photocurrent hysteresis during operation.[4,18–20] Various explanations have been suggested and the most popular one assumes ferroelectricity stemming from the dipolar properties of the organic group.[21] Current–voltage (*i–V*) sweep curves collected from $MAPbI_3$ single crystals displayed a non-Ohmic, hysteretic behavior,[22] which resembles a ferroelectric loop. Yet the anomalies under regard appeared at frequencies that are much lower than expected for ferroelectricity. Indeed previous dielectric studies for $MAPbI_3$ revealed that the MA dipoles are fully disordered with relaxation on a picosecond time scale at room temperature.[23,24]

A few prior studies have linked these processes tentatively and very vaguely to the dynamics of slow charge carriers with a time constant in the range of milliseconds to seconds.[4,17] However, the nature of such slow charge carriers have not been identified so far, neither have systematic studies in that respect been performed.

In this letter, we 1) separate electronic and ionic conductivities, 2) show the significance of ionic conduction, 3) identify it as iodine conduction, and 4) study implications of the mixed electronic/ionic nature of these materials. Sandwiching such a mixed conductor between neighboring phases that allow for electronic transport but block the ionic transport, as it is the case for photovoltaic applications, results in a stoichiometric polarization that can largely explain the above anomalies. This unavoidable process is related to a chemical capacity C^{δ}[25–27] rather than a dielectric phenomenon and appears in various contexts under the names of Wagner–Hebb[28] or Yokota polarization.[29,30] In the non-linear range this phenomenon is also known as resistance degradation[31] or electrocoloration.[32] Indeed, related perovskites such as $CsPbI_3$, $CsPbBr_3$ or $MAGeCl_3$, $MASnCl_3$ are known to be halide ion conductors,[33–35] and Xiao et al. have demonstrated ion migration under electric field in $MAPbI_3$.[36]

Moreover, as the electrical properties of organic–inorganic lead-halide-based perovskites have been shown to be affected by the size of the organic cation occupying the A site, we investigate here also how the ionic and the electronic conductivities change as a function of the gradual substitution of MA with formamidinium ($HN=CHNH_3^+$, FA) in $MA_{1-x}FA_xPbI_3$. This is particularly relevant since according to our previous study,[37] this variation can be correlated with the photoelectrical performance.

The electrical properties of $MAPbI_3$ were investigated under argon and in the dark (compare the Supporting Information). Typical alternating-current (AC) impedance spectra acquired from $MAPbI_3$ pellets using graphite electrodes consist of a single distorted semicircle (Figure 1 a). Owing

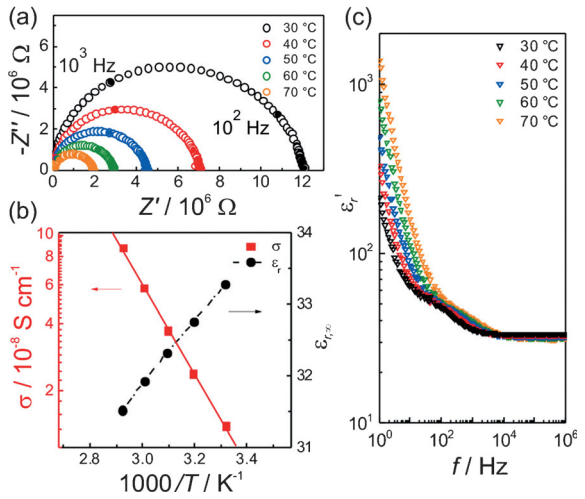

Figure 1. a) AC impedance spectra acquired from $MAPbI_3$ pellets from 1 MHz to 1 Hz. The solid symbols correspond to data acquired at 1 kHz and 100 Hz, respectively. b) Temperature dependence of the conductivity σ and the bulk relative dielectric constant $\varepsilon_{r,\infty}$. c) The real part of the complex permittivity ε'_r as a function of frequency.

to the calculated relative dielectric constant, this feature can be assigned to the pure bulk properties ($\varepsilon_{r,\infty}=34$ at 30 °C).[38] The value of $\varepsilon_{r,\infty}$ slightly decreases with increasing temperature (Figure 1 b). Though not small, neither the absolute values nor the temperature dependence of the dielectric constant suggest ferroelectricity. This is in keeping with previous dielectric measurements that show ferroelectric behavior of $MAPbI_3$ to appear only below the temperature of the tetragonal-to-orthorhombic transition at 162 K.[23] Blocking effects stemming from grain boundaries are not observed.

The bulk conductivity increases with temperature (Figure 1 b) with an activation energy of 0.43 eV, in agreement with previous literature.[39] As shown in Figure 1 c, the real part of the complex permittivity (ε'_r) for high frequencies ($>10^4$ Hz) is slightly reduced as temperature increases. In the lower frequency range, ε'_r begins to rapidly rise by an order of magnitude up to 300 at 1 Hz and 30 °C (at 10 mHz ε'_r reaches values up to 10^4, see the Supporting Information). These high values of ε'_r at low frequencies increase with increasing temperature. Such a behavior resembles what Juarez-Perez et al. observed from $MAPbI_3$-containing solar cells.[16] We show in detail that this is the natural consequence of a stoichiometric polarization occurring when the perovskite is sandwiched in between contacts that block the ions. Galvanostatic direct current (DC) measurements using—for this purpose—graphite electrodes clearly reveal the mixed conducting (i.e. ionic as well as electronic) behavior, as depicted in Figure 2 a. In a typical experiment, upon switching

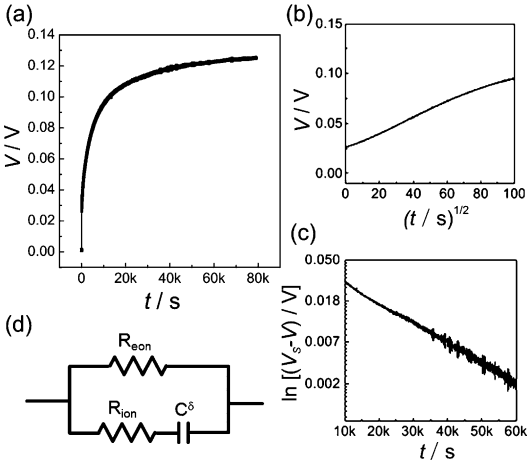

Figure 2. a) DC polarization curve for a C | $MAPbI_3$ | C cell measured at 30 °C in Ar flow by applying a current of 2 nA. b) Voltage versus square root of time up to 10^4 seconds. c) Semi-log plot of voltage versus time at longer time scale. d) Equivalent circuit mimicking the DC polarization (R_{eon}: electronic resistance, R_{ion}, ionic resistance, C^δ: chemical capacitance). The equivalent circuit fails in describing the $\sqrt{t}$ behavior. Here the general transmission line circuit has to be used.

on the current ($i=2$ nA), the voltage instantaneously reaches 25 mV; This iR drop corresponds to the total electrical resistance (12.5 MΩ), to which both electrons and ions contribute $V=i(R_{eon}R_{ion}/(R_{eon}+R_{ion}))$, compare Figure 2 d. This value is consistent with the resistance derived from the impedance spectra. As the duration of the current load increases, ions are progressively blocked giving rise to an internal compositional gradient. As a consequence, the voltage also increases and reaches the saturation value V_s. In the steady state, only electrons flow ($i=i_{eon}, i_{ion}=0$) leading to $V_s=iR_{eon}$. Note that this is a standard experiment in solid-state electrochemistry to separate ionic and electronic conductivities.[40,41]

From V_s, the electronic conductivity (σ_{eon}) follows as 1.9×10^{-9} S cm^{-1} and hence the ionic conductivity as 7.7×10^{-9} S cm^{-1} ($\sigma_{tot}=\sigma_{ion}+\sigma_{eon}$). Quite remarkably, in dark condition $\sigma_{ion}>\sigma_{eon}$. However, during exposure to a 150 W halogen lamp, σ_{eon} clearly greatly increases owing to the photogeneration of charge carriers, while σ_{ion} appears to be less sensitive to the illumination (Figure S7).

The investigation of the transient further proves that the observed polarization is due to a chemical diffusion process. As predicted for chemical diffusion,[30,40] the transient curve fits a $\sqrt{t}$ law for short times (i.e. for $t<\tau^\delta$, with $\tau^\delta=R^\delta C^\delta$ being the polarization time constant), and for longer time ($t>\tau^\delta$) an exponential behavior. Figure 2 b and c show that both time dependences are excellently verified with practically identical

τ^δ values of 1.6×10^4 s and 2.1×10^4 s, respectively. This remarkable agreement is, besides the successful verification of the predicted analytical form of the voltage transient, a very strong argument for chemical diffusion. From τ^δ, the chemical diffusion coefficient of the mobile ion ($D^\delta = L^2/(\pi^2\tau^\delta)$ with L being the sample thickness) is found to be 2.4×10^{-8} cm^{2}s^{-1}.

Even though the voltage evolution leaves no doubt on the mixed conducting nature with predominant ionic contribution, we obtained further irrefutable evidence based on another standard technique to separate ionic and electronic conductivities, namely the open circuit voltage (V_{OC}) under a chemical potential gradient. We produce the potential gradient under electrolysis conditions (we expect formation of lead on one and of iodine on the other side). The open circuit potential after switching off the current is 788 mV, which is about 100 mV lower than the standard potential for forming PbI_2 from Pb and I_2 (899 mV). A predominantly electronic conductor would yield a V_{OC} close to zero. The finite electronic transport leads to an internal chemical short circuit, that is, to a reversal of the electrolysis process and hence to a V_{OC} decay on the time scale of tens of hours. Again, this time scale fits to the derived conductivity of the minority charge carriers (see Figure S5 for details).

To even further safe-guard this result, we set up stationary chemical potential gradients using two galvanic cells, that is, (Pb,PbI_2) | $MAPbI_3$ | (Ag,AgI) and (Pb,PbI_2) | $MAPbI_3$ | (Cu,CuI). In both cases the V_{OC} is found to be approximately 50–60 % of the Nernst value given by $\{\Delta_f G(PbI_2) - 2\Delta_f G(\text{AgI or CuI})\}/2F$ ($\Delta_f G$ being the molar Gibbs energy of formation and F the Faraday constant). This value is in good agreement with the polarization results (Figure S6). A predominant electronic conductor would yield a V_{OC} value close to zero. The measured transference number also matches the values estimated from the electrolysis, as the decomposition voltage of the organic–inorganic halide should be higher than that of PbI_2.

Although this verification of the ionic conductivity suffices to explain the observed anomalies, we have sought to determine the nature of the conducting ion. For this purpose, a solid-state electrochemical cell consisting of Pb | $MAPbI_3$ | AgI | Ag was employed (Figure 3a). Such a coulometric cell configuration with one electronic (Pb) and one ionic electrode (AgI | Ag) causes chemical changes on current flow. The investigation of chemical effects at the various interfaces A, B, C, and D (Figure 3a) upon long-term charge transference (the Pb electrode taken as plus and the Ag electrode as minus pole) allows for the identification of the moving ions. Specifically, if Pb^{2+} is mobile, PbI_2 is formed at the interface C. However, if the anion I^- is the fastest moving species, then it can react with Pb and form PbI_2 at the interface B. If MA^+ is mobile, MAI and PbI_2 are formed at interfaces C and B, respectively.

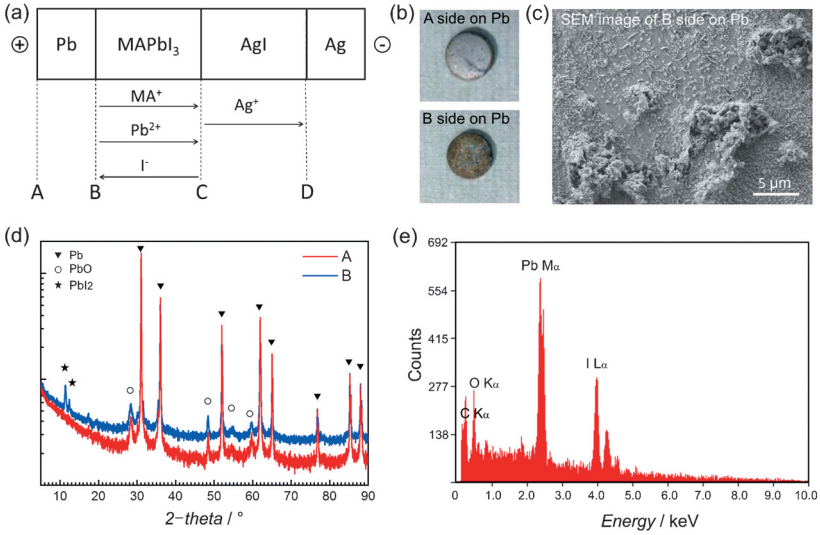

Figure 3. a) Flow directions of the charged ion species in a Pb | $MAPbI_3$ | AgI | Ag cell under electrical bias. b) Images for surfaces A and B and c) a scanning electron microscope (SEM) image of surface B on the Pb pellet. d) XRD patterns of surfaces A and B of the Pb disk after applying a DC current of 10 nA for a week. e) EDS spectrum for surface B of Pb.

Having set-up such a cell, a DC current of 10 nA was applied for a week at 50 °C in Ar atmosphere and subsequently the surfaces of the Pb disk were inspected. As displayed in Figure 3b, while the surface of interface A maintained the original morphology and Pb appearance, the surface of interface B exhibited a yellowish color and a perceptible roughness. In the SEM micrograph (Figure 3c), the formation of grains with irregular shape at the B interface could be recognized on the originally smooth Pb surface. The other disks ($MAPbI_3$ as well as AgI) did not reveal any change upon the test.

Their composition was examined by energy dispersive X-ray spectroscopy (EDX) and X-ray diffraction (XRD). EDX spectra acquired from the agglomerates revealed the presence of Pb and I signals (Figure 3e), from which an atomic I-to-Pb ratio of 2.2 results, while XRD patterns showed the presence of a secondary phase (see in Figure 3d the additional peaks at $2\theta = 11.4°$ and 12.4°, respectively). As the peak at 12.4° can be assigned to PbI_2, both XRD and EDX analyses indicate I^- to easily migrate through $MAPbI_3$, meaning that the stoichiometric polarization shown in Figure 2 results from the iodine ion conduction. To make sure that this is not an artifact of a local reaction, we tested the same cell configuration under the same ambient conditions without applying a current. The result was negative indicating local chemical stability (Figure S10). This behavior is very similar to that of $CsPbI_3$.[33]

As the ionic carrier mobility hardly exceeds 10^{-2} cm^{-2}V^{-1}s^{-1} in ionic crystals at room temperature and the mobility of the electronic carriers is reported to be more than three orders of magnitude higher,[22,42] the disorder in such a mixed conductor must be primarily ionic (i.e. the ionic charge carrier concentration exceeds that of the electrons by far). The typical defect chemical situation in perovskites is characterized by Schottky disorder. Here a variety of possibilities comes into question, the most probable being an understoichiometry owing to a deficiency of (MA)I.[43]

Another realistic situation is an extrinsic one dominated by O'_I defects (oxygen substituting for iodine). In all these cases the major iodine defect is the iodine vacancy $V^{\bullet}_I$. The complexity is increased by the possibility of also having iodine interstitials. This is rather unexpected for perovskites from size considerations but suggested by atomistic modeling.[14,15] In this case the electronic concentration would be kept small by trapping of holes by iodine interstitials.[44,45] In the other cases, trapping by O'_I, V'_{MA}, V''_{Pb} is to be considered. Fortunately these details are not decisive for our rationale so that it suffices to refer to the most mobile iodine defect ($V^{\bullet}_I$ or I'_I) as "ion" and the most mobile electronic defect ($h^{\bullet}$) as "eon".[46]

Now let us analyze the chemical diffusion coefficient. Under general conditions it can be written as Equation (1),[47]

$$D^{\delta} = \frac{\sigma_{eon}}{\sigma_{ion}+\sigma_{eon}} D_{ion}\chi_{ion} + \frac{\sigma_{ion}}{\sigma_{ion}+\sigma_{eon}} D_{eon}\chi_{eon} \quad (1)$$

where χ_{ion} and χ_{eon} denote the respective differential trapping factors, and D_{ion} and D_{eon} are the individual diffusivities being proportional to the respective mobility. As $D_{eon} \gg D_{ion}$ this can be simplified for the predominantly ionic conducting material to $D^{\delta} = D_{eon}\chi_{eon}$. Without trapping ($\chi_{eon} = 1$) this result would largely contradict the experimental observations, as D_{eon} is expected to be on the order of 10^{-1} cm^2 s^{-1},[22] which is seven orders of magnitude larger than the observed D^{δ} value. If, however, strong trapping plays a key role,[48] the observed low value is directly explained. Such an exothermic trapping is rather the rule than the exception at room temperature. It is shown in Section S4 of the Supporting Information, that if χ_{ion} dominates the electrical transport properties (as in the present case under dark conditions), then Equation (2)

$$D^{\delta} = D_{eon}[h^{\bullet}]/[T^{x}] \quad (2)$$

results (rather than $D^{\delta} = D_{eon}$), with $[T^x]$ being the concentration of trapped holes (occupied traps). This directly explains the magnitude of D^{δ} by the small fraction of free holes.[22]

To clarify most straightforwardly that the stoichiometric polarization necessarily occurring in photovoltaic applications is relevant 1) for the observed dielectric anomaly and 2) for the hysteresis in photocurrent–voltage curves, we use the fact that such a stoichiometric polarization can be approximately described by the equivalent circuit given in Figure 2d with the chemical capacitance C^{δ} blocking the ionic resistor R_{ion} in the steady state. We do this only for the purpose of simplifying the presentation. The relation between the equivalent circuit representation and the exact treatment based on irreversible thermodynamics is set out in detail in Ref. [49]. An equivalent circuit describing the polarization more accurately is given in Refs. [26] and [50].

1) First we attribute the permittivity anomaly to the stoichiometric polarization, the transient of which is characterized by Equation (3) (see Ref. [51]).

$$C^{\delta} = \frac{\tau^{\delta}}{R^{\delta}} = \tau^{\delta}\sigma^{\delta}\frac{A}{L} = \frac{AL}{\pi^2}\frac{\sigma^{\delta}}{D^{\delta}} \propto AL[T^{x}] \quad (3)$$

A is the cross-sectional area of the samples, and $R^{\delta} = R_{ion} + R_{eon}$. The chemical resistance R^{δ} is determined by the inverse of the ambipolar conductivity σ^{δ}, which is given by $\sigma_{ion}\sigma_{eon}/(\sigma_{ion}+\sigma_{eon})$. The chemical capacitance is hence dominated by the density of the trapped holes (occupied traps). Inserting the parameters from Figure 2, we derive $C^{\delta} = 2.3\times10^{-4}$ F corresponding to an apparent $\varepsilon'_r = 3.6\times10^{8}$. This huge but typical value explains the rise of ε'_r in the low frequency range, even prior to a distinct Warburg feature. The analysis of $\varepsilon'_r(\omega)$ based on the interpretation of the equivalent circuit of Figure S8 reveals that $\varepsilon'_r(\omega)$ depends on the ionic conductance and the chemical capacitance only; σ_{eon} is solely of importance in the range of the $\sqrt{t}$ law.

The next question to be answered is how to explain the increase of ε'_r on illumination. As illumination increases the electronic carrier concentration, we also expect an increase of the concentration of occupied traps yielding a larger C^{δ}. A closer analysis reveals that, apart from the Warburg range, ε'_r is solely determined by R_{ion} and C^{δ}. The saturation value $\varepsilon'_r(\omega = 0)$ (compare Section S6) is directly determined by C^{δ}. The modeling described in detail in the Supporting Information reveals that the best fit of the experimental results is obtained if R_{ion} decreases and C^{δ} increases on illumination. While the increase of C^{δ} is expected, the decrease of R_{ion} instead is surprising and deserves a closer look in future research, in particular as preliminary measurements of ours indeed give evidence for such an effect (Figure S7). Note that (unlike the hysteresis, see below) the ε'_r anomaly also appears for predominant electronic conduction.

2) Also the hysteresis in a cyclic sweep experiment on perovskite solar cells under illumination can be ascribed to the stoichiometric polarization. As shown in Figure 4a, as-prepared $MAPbI_3$ pellets showed a non-Ohmic behavior and a clear hysteresis loop when the DC current was swept between -20 and $+20$ nA. This behavior is the direct consequence of stoichiometric polarization, which can be directly verified by using the aforementioned equivalent circuit (compare Section S5). To further test our interpretation, we measured the i–V sweep curve of $MAPbI_3$ treated in an atmosphere of high iodine partial pressure. This sample was predominantly electronically conducting and did not exhibit stoichiometric polarization. Indeed, the corresponding i–V sweep shows a purely Ohmic behavior without perceptible hysteresis (Figure 4c). The same happens when oxygen traces are incorporated into the material generating holes. This can explain the disappearance of hysteresis observed for samples that have seen ambient conditions at elevated temperature.[52]

The extent of the hysteresis is affected by the sweep rate μ ($i = \mu t$). As μ increases, the hysteresis loop is expected to widen when $\tau^{\delta} \ll t_u$, with t_u being the reversal time, while it narrows when $\tau^{\delta} > t_u$ (compare the Supporting Information for the details). Both cases were observed in i–V sweeps of perovskite solar cells,[18,19] which can be attributed to variations in τ^{δ}, while in our experiments only the last case is met (Figure 4b), where $\tau^{\delta} \approx 10^4$ s and $t_u = 4$ s (2000 s) for $\mu =$ 5 nA s^{-1} (0.01 nA s^{-1}). On illumination the hysteresis becomes less pronounced if $t_u \gg \tau^{\delta}$ (note that the extent of the hysteresis is proportional to $R_{eon}{}^2 C^{\delta} \propto (1/c_{eon})$ and disappears

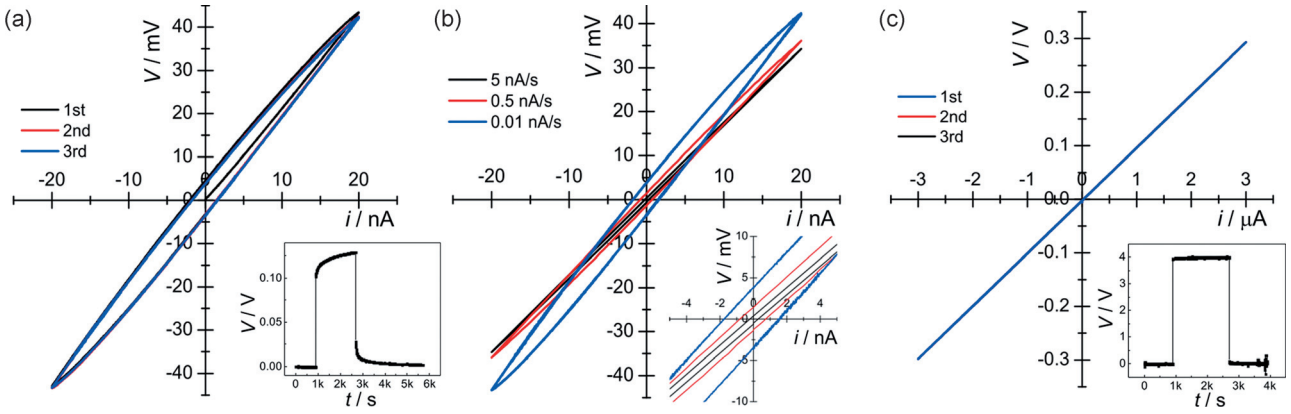

Figure 4. Current–voltage curves for $MAPbI_3$. Hysteresis loops upon the current sweep a) between −20 nA and 20 nA with the rate of 0.01 nA s^{-1} and b) with varying the scan rate. As shown in the inset in (a), the samples showing the hysteretic behavior exhibit mixed (ionic and electronic) conductivity. The inset of (b) clearly illustrates the changes of the open circuit voltage when the current sweep rate is changed. c) Current–voltage curve for $MAPbI_3$ that did not show the stoichiometric polarization by controlling the atmosphere. As shown in the inset this sample exhibit only electronic transport.

for $\sigma_{eon} \gg \sigma_{ion}$). Yet it is important to repeat that in these cases the low-frequency anomaly in ε'_r remains.

Finally, it is worth considering the above phenomena with regard to thin films or perovskite infiltrated in mesoporous titania.[18] Here both C^δ and τ^δ are distinctly smaller: Both $\varepsilon'_r(\omega=0)$ as well as τ^δ are proportional to L^2 (L being the diffusion length) and hence substantially lowered, which leads to a quicker polarization and lower apparent ε'_r at low frequencies. On illumination τ^δ decreases further, while $\varepsilon'_r(\omega=0)$ increases. This explains why the hysteresis in the solar cell narrows with decreasing μ (corresponding to $\tau^\delta \ll t_u$).[18] As the width of the hysteresis is proportional to $R_{eon}{}^2 C^\delta \propto L^3$, we expect a decreased hysteresis for thinner films. Moreover, in very thin films, space-charge-dominated zones can play an important role and the whole picture becomes more involved.

In Ref. [37] it was shown that crystals with a mixture of methylammonium (MA) and formamidinium (FA) on A-sites shows a efficiency maximum for 60 at.% MA because of a longer lifetime of photogenerated carriers. Since bulk ionic and electronic transport can be affected by the lattice distortion in lead halide octahedra, it is worth investigating whether the iodine migration depends on the mixing ratio.

Figure 5a depicts σ_{ion} and σ_{eon} for $MA_{1-x}FA_xPbI_3$ as x increases from 0 to 1. Strikingly, the values vary by one or two orders of magnitude with particularly high values for intermediate compositions. The highest σ_{ion} is measured for $MA_{0.4}FA_{0.6}PbI_3$ for which it surpasses σ_{eon} by one order of magnitude. Unsurprisingly, the electronic conductivity itself is less sensitive with respect to the A-site cation, than the ionic conductivities.

The chemical diffusion coefficient D^δ of the ionic charge carrier is calculated by fitting the exponential part of the DC polarization curve as described above in Figure 2a. D^δ increases with increasing FA fraction up to $x=0.4$ and then remains constant. The trend of the chemical diffusion coefficient is qualitatively similar to that of σ_{eon} indicating, according to Equation (3), a roughly constant concentration of occupied traps. If the trapping energies are not significantly altered and the total trap density is roughly invariant, the enhanced lifetime of photogenerated carriers at $MA_{0.6}FA_{0.4}PbI_3$[37] may be attributed to a maximum electronic mobility.

In summary, we have demonstrated the significance of ionic transport in organic lead-iodide-based perovskites. Notably, in $MAPbI_3$, the ionic conductivity is found to be higher than the electronic conductivity. The large ionic transference number points towards high native ionic disorder and substantial trapping of the electronic carriers. The

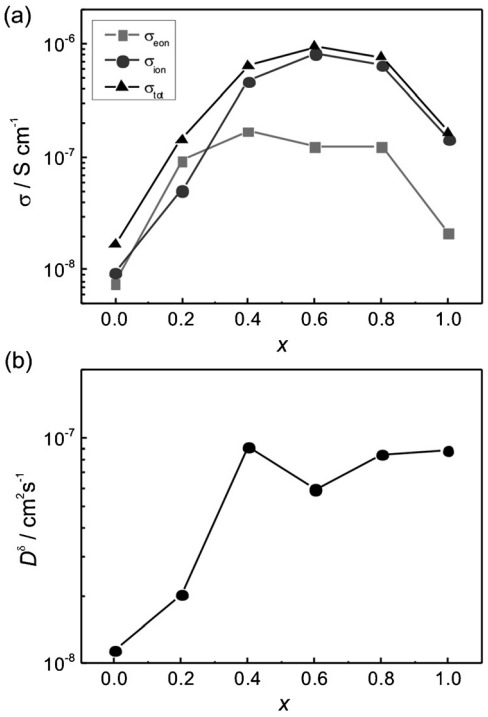

Figure 5. Electrical transport properties of mixed-cation lead iodide, $MA_{1-x}FA_xPbI_3$. a) Changes of electronic, ionic, and total conductivities as a function of the FA faction x and b) chemical diffusion coefficients for the same compositions.

stoichiometric polarization can explain both the large value of the apparent dielectric constant occurring at low frequencies as well as the hysteresis in the cyclic sweep experiments. The same features also explain the trend of chemical diffusivities and partial conductivities on substituting MA by FA ($MA_{1-x}FA_xPbI_3$). It will be a future task to elucidate to what extent stoichiometric definition is able to improve operation as well as to what extent ionic motion may be beneficial for the photoelectrochemical activity.

Keywords: dielectric constant · hysteresis · ionic conduction · perovskite solar cells · polarization

How to cite: *Angew. Chem. Int. Ed.* **2015**, *54*, 7905–7910
Angew. Chem. **2015**, *127*, 8016–8021

[1] K. Tanaka, T. Takahashi, T. Ban, T. Kondo, K. Uchida, N. Miura, *Solid State Commun.* **2003**, *127*, 619–623.
[2] G. C. Papavassiliou, G. A. Mousdis, I. B. Koutselas, *Adv. Mater. Opt. Electron.* **1999**, *9*, 265–271.
[3] G. Xing, N. Mathews, S. Sun, S. S. Lim, Y. M. Lam, M. Grätzel, S. Mhaisalkar, T. C. Sum, *Science* **2013**, *342*, 344–347.
[4] A. Dualeh, T. Moehl, N. Tétreault, J. Teuscher, P. Gao, M. K. Nazeeruddin, M. Grätzel, *ACS Nano* **2013**, *8*, 362–373.
[5] I. Borriello, G. Cantele, D. Ninno, *Phys. Rev. B* **2008**, *77*, 235214.
[6] A. Kojima, K. Teshima, Y. Shirai, T. Miyasaka, *J. Am. Chem. Soc.* **2009**, *131*, 6050–6051.
[7] J. M. Ball, M. M. Lee, A. Hey, H. J. Snaith, *Energy Environ. Sci.* **2013**, *6*, 1739–1743.
[8] J. Burschka, N. Pellet, S.-J. Moon, R. Humphry-Baker, P. Gao, M. K. Nazeeruddin, M. Gratzel, *Nature* **2013**, *499*, 316–319.
[9] H. S. Kim, C. R. Lee, J. H. Im, K. B. Lee, T. Moehl, A. Marchioro, S. J. Moon, R. Humphry-Baker, J. H. Yum, J. E. Moser, M. Grätzel, N. G. Park, *Sci. Rep.* **2012**, *2*, 591.
[10] J. H. Noh, S. H. Im, J. H. Heo, T. N. Mandal, S. I. Seok, *Nano Lett.* **2013**, *13*, 1764–1769.
[11] S. Ryu, J. H. Noh, N. J. Jeon, Y. Chan Kim, W. S. Yang, J. Seo, S. I. Seok, *Energy Environ. Sci.* **2014**, *7*, 2614–2618.
[12] S. D. Stranks, G. E. Eperon, G. Grancini, C. Menelaou, M. J. P. Alcocer, T. Leijtens, L. M. Herz, A. Petrozza, H. J. Snaith, *Science* **2013**, *342*, 341–344.
[13] C. Wehrenfennig, G. E. Eperon, M. B. Johnston, H. J. Snaith, L. M. Herz, *Adv. Mater.* **2014**, *26*, 1584–1589.
[14] W.-J. Yin, T. Shi, Y. Yan, *Appl. Phys. Lett.* **2014**, *104*, 063903.
[15] M. H. Du, *J. Mater. Chem. A* **2014**, *2*, 9091–9098.
[16] E. J. Juarez-Perez, R. S. Sanchez, L. Badia, G. Garcia-Belmonte, Y. S. Kang, I. Mora-Sero, J. Bisquert, *J. Phys. Chem. Lett.* **2014**, *5*, 2390–2394.
[17] R. S. Sanchez, V. Gonzalez-Pedro, J.-W. Lee, N.-G. Park, Y. S. Kang, I. Mora-Sero, J. Bisquert, *J. Phys. Chem. Lett.* **2014**, *5*, 2357–2363.
[18] N. J. Jeon, J. H. Noh, Y. C. Kim, W. S. Yang, S. Ryu, S. I. Seok, *Nat. Mater.* **2014**, *13*, 897–903.
[19] H. J. Snaith, A. Abate, J. M. Ball, G. E. Eperon, T. Leijtens, N. K. Noel, S. D. Stranks, J. T. W. Wang, K. Wojciechowski, W. Zhang, *J. Phys. Chem. Lett.* **2014**, *5*, 1511–1515.
[20] E. L. Unger, E. T. Hoke, C. D. Bailie, W. H. Nguyen, A. R. Bowring, T. Heumuller, M. G. Christoforo, M. D. McGehee, *Energy Environ. Sci.* **2014**, *7*, 3690–3698.
[21] J. M. Frost, K. T. Butler, F. Brivio, C. H. Hendon, M. van Schilfgaarde, A. Walsh, *Nano Lett.* **2014**, *14*, 2584–2590.
[22] C. C. Stoumpos, C. D. Malliakas, M. G. Kanatzidis, *Inorg. Chem.* **2013**, *52*, 9019–9038.
[23] N. Onoda-Yamamuro, T. Matsuo, H. Suga, *J. Phys. Chem. Solids* **1992**, *53*, 935–939.
[24] A. Poglitsch, D. Weber, *J. Chem. Phys.* **1987**, *87*, 6373–6378.
[25] J. Bisquert, *Phys. Chem. Chem. Phys.* **2003**, *5*, 5360–5364.
[26] J. Jamnik, J. Maier, *J. Electrochem. Soc.* **1999**, *146*, 4183–4188.
[27] J. Maier, *Z. Phys. Chem.* **1984**, *140*, 191–215.
[28] M. H. Hebb, *J. Chem. Phys.* **1952**, *20*, 185–190.
[29] I. Yokota, *J. Phys. Soc. Jpn.* **1953**, *8*, 595–602.
[30] I. Yokota, *J. Phys. Soc. Jpn.* **1961**, *16*, 2213–2223.
[31] T. Baiatu, R. Waser, K.-H. Härdtl, *J. Am. Ceram. Soc.* **1990**, *73*, 1663–1673.
[32] J. Blanc, D. L. Staebler, *Phys. Rev. B* **1971**, *4*, 3548–3557.
[33] J. Mizusaki, K. Arai, K. Fueki, *Solid State Ionics* **1983**, *11*, 203–211.
[34] K. Yamada, K. Isobe, E. Tsuyama, T. Okuda, Y. Furukawa, *Solid State Ionics* **1995**, *79*, 152–157.
[35] K. Yamada, Y. Kuranaga, K. Ueda, S. Goto, *Bull. Chem. Soc. Jpn.* **1998**, *71*, 127–127.
[36] Z. Xiao, Y. Yuan, Y. Shao, Q. Wang, Q. Dong, C. Bi, P. Sharma, A. Gruverman, J. Huang, *Nat. Mater.* **2015**, 14, 193–198.
[37] N. Pellet, P. Gao, G. Gregori, T.-Y. Yang, M. K. Nazeeruddin, J. Maier, M. Grätzel, *Angew. Chem. Int. Ed.* **2014**, *53*, 3151–3157; *Angew. Chem.* **2014**, *126*, 3215–3221.
[38] F. Brivio, A. B. Walker, A. Walsh, *APL Mater.* **2013**, *1*, 042111.
[39] O. Knop, R. E. Wasylishen, M. A. White, T. S. Cameron, M. J. v. Oort, *Can. J. Chem.* **1990**, *68*, 412.
[40] J. Maier, *Physical chemistry of ionic materials*, Wiley, Chichester, **2004**, pp. 444–460.
[41] *Solid state chemistry* (Ed.: P. G. Bruce), University Press Cambridge, Cambridge, **1997**.
[42] D. B. Mitzi, *J. Chem. Soc. Dalton Trans.* **2001**, 1–12.
[43] A. Walsh, D. O. Scanlon, S. Chen, X. G. Gong, S.-H. Wei, *Angew. Chem. Int. Ed.* **2015**, *54*, 1791–1794; *Angew. Chem.* **2015**, *127*, 1811–1814.
[44] M. Samiee, S. Konduri, B. Ganapathy, R. Kottokkaran, H. A. Abbas, A. Kitahara, P. Joshi, L. Zhang, M. Noack, V. Dalal, *Appl. Phys. Lett.* **2014**, *105*, 153502.
[45] S.-H. Duan, H. Zhou, Q. Chen, P. Sun, S. Luo, T.-B. Song, B. Bob, Y. Yang, *Phys. Chem. Chem. Phys.* **2015**, *17*, 112–116.
[46] If Refs. [14] and [15] are right in that for all easily formable defects the ionization energy is very small, we might have to refer to extrinsic defects such as substitutional oxygen impurities to efficiently capture the holes (close to the valence band). However, already slightly higher energies that are within the accuracy of such modeling can lead to substantial trapping, if the number of trap centers is very high, as it is the case for ionic disorder. So also intrinsic defects cannot be excluded as trap centers.
[47] J. Maier, *J. Am. Ceram. Soc.* **1993**, *76*, 1212–1217.
[48] J. Maier, R. Amin, *J. Electrochem. Soc.* **2008**, *155*, A339–A344.
[49] J. Jamnik, J. Maier, *Phys. Chem. Chem. Phys.* **2001**, *3*, 1668–1678.
[50] J. Jamnik, J. Maier, *Ber. Bunsen-Ges.* **1997**, *101*, 23–40.
[51] J. Maier, *Solid State Phenom.* **1994**, *39–40*, 35–60.
[52] W. Nie, H. Tsai, R. Asadpour, J. C. Blancon, A. J. Neukirch, G. Gupta, J. J. Crochet, M. Chhowalla, S. Tretiak, M. A. Alam, H. L. Wang, A. D. Mohite, *Science* **2015**, *347*, 522–525.

Received: January 3, 2015
Revised: March 17, 2015
Published online: May 15, 2015

